metals

MDPI

Article

Hydrogen Embrittlement Behavior of a Commercial QP980 Steel

Linlin Zhao [1,2], Cheng Ma [2,*], Aimin Zhao [1,*], Yuheng Fan [3,*] and Zhiqiang Li [3]

[1] Collaborative Innovation Center of Steel Technology, University of Science and Technology Beijing, Beijing 100083, China; zhaolinlin@hbisco.com
[2] Materials Technology Research Institute, HBIS Group, Shijiazhuang 050000, China
[3] School of Materials Science and Engineering, Zhengzhou University, Zhengzhou 450001, China
* Correspondence: macheng01@hbisco.com (C.M.); zhaoaimin@ustb.edu.cn (A.Z.); yhfan@zzu.edu.cn (Y.F.)

Abstract: The hydrogen embrittlement (HE) behavior of a commercial QP980 steel is studied in this work. The HE susceptibility results indicate that QP980 suffers from a severe HE, and the fracture mode transforms from ductile dimpling to brittle quasi-cleavage under the attack of hydrogen. The EBSD results show that strain-induced martensite transformation can rarely occur at a strain close to the HE fracture strain, which is mainly attributed to the high mechanical stability of austenite. The TKD-KAM analysis results indicate that hydrogen-induced strain localization in martensite can be mitigated by the hydrogen-trapping effect of surrounding austenite, while it is most pronounced in martensite adjacent to ferrite. Correspondingly, HE cracking is considered to initiate in martensite adjacent to ferrite under the synergistic action of HELP and HEDE mechanisms, and then cracks can propagate through ferrite or along phase interfaces. Our findings suggest that to further improve the HE resistance of QP steel with stable austenite, it is necessary to consider introducing effective hydrogen-trapping sites (such as carbides, film austenite) into martensite, which is deemed to be beneficial for increasing the resistance against hydrogen-induced cracking initiation in martensite.

Keywords: QP steel; hydrogen embrittlement; TKD; SEM

check for updates

Citation: Zhao, L.; Ma, C.; Zhao, A.; Fan, Y.; Li, Z. Hydrogen Embrittlement Behavior of a Commercial QP980 Steel. *Metals* **2023**, *13*, 1469. https://doi.org/10.3390/met13081469

Academic Editors: John Campbell and Hardy Mohrbacher

Received: 6 July 2023
Revised: 4 August 2023
Accepted: 14 August 2023
Published: 15 August 2023

Copyright: © 2023 by the authors. Licensee MDPI, Basel, Switzerland. This article is an open access article distributed under the terms and conditions of the Creative Commons Attribution (CC BY) license (https://creativecommons.org/licenses/by/4.0/).

1. Introduction

Quenching and partitioning (QP) steels, as third-generation advanced high-strength steels (AHSSs), have been extensively utilized in various critical applications, including automotive and aerospace industries, due to their outstanding mechanical properties, such as high strength, excellent toughness, and good ductility [1,2]. The microstructure of QP steels is mainly composed of carbon-enriched retained austenite (RA), carbon-depleted martensite and ferrite in the case of intercritical annealing [3], and the transformation-induced plasticity (TRIP) effect induced by austenite upon deformation is deemed to contribute to the favorable ductility of QP steels [4].

However, in practical applications, hydrogen can be introduced into QP steel from various sources, including environmental exposure, hydrogen-containing fluids, or even during the steel production process itself, which leads to a premature failure of QP steels, i.e., hydrogen embrittlement (HE). In the literature, QP steels have been proven to suffer from sever HE, accompanying a transition of the fracture mode from ductile dimpling to brittle intergranular or quasi-cleavage fracturing [5–7]. Up to now, many mechanisms with respect to HE were proposed in previous studies, such as hydrogen-enhanced localized plasticity (HELP, proposing that hydrogen facilitates dislocation activity and promotes planar slip) [8], hydrogen-enhanced decohesion (HEDE, where hydrogen causes a reduction in the cohesive bond strength) [9], adsorption-induced dislocation emission (AIDE, where hydrogen adsorption accelerates dislocation emissions at the crack tip) [10] and hydrogen-enhanced strain-induced vacancies (HESIV, where the strain-induced generation of vacancies is enhanced in the presence of hydrogen) [11]. The critical mechanism

accounting for a specific HE fracture is generally determined via scanning electron microscopy (SEM) analysis of the fracture surface or transmission electron microscope (TEM) observations of the microstructure immediately beneath the fracture surface [12,13], and a synergistic action of the above mechanisms may exist rather than a single one [14].

Generally, the HE fracture is closely related to the hydrogen's fugacity and the microstructure. It has been reported that hydrogen-induced cracking normally occurs when the hydrogen concentration exceeds a critical value. However, it should be noted that hydrogen is rarely homogeneously distributed in steels due to the different hydrogen solubility and trapping capacity of various phases, and thus how hydrogen is distributed in steel can have a huge influence on the HE susceptibility of steels. For instance, by introducing carbides in high-strength martensitic steel, the HE is effectively relieved since hydrogen in the matrix decreases due to the hydrogen-trapping effect of carbides [13]. As for QP steel with a multi-phase structure, the hydrogen distribution is heterogeneous in different phases, which should be considered when studying the HE mechanism of QP steels.

In addition, it has been found that various microstructures show quite different susceptibilities to HE. For QP steels, martensite, as a hard phase, is considered to be most sensitive to HE, while ferrite, as a soft phase, is considered to be less susceptible to HE [15]. However, as for RA, how it influences the HE is still controversial. On the one hand, RA has a lower hydrogen diffusion rate and a higher hydrogen solubility than martensite/ferrite, and is considered to provide hydrogen-trapping sites, leading to an increase in HE resistance [16,17]. On the other hand, RA may serve as a "source" of hydrogen after deformation-induced martensite transformation and can accelerate the HE failure [18,19]. The reasons for the above conflicting arguments are usually ascribed to the mechanical stability of RA, which is considered to be related to the chemical composition and morphology of RA. For example, RA films with a higher mechanical stability are reported to be much more immune to HE than blocky ones with a lower mechanical stability, and HE cracking is more likely to occur in blocky RA [5].

It should be also noted that a heterogenous distribution of strain (i.e., strain localization) can exist during the deformation of QP steel owing to the inherent mechanical property differences among various constituent phases [20], and cracking is apt to occur at the region with high localized strain. Under the attack of hydrogen, the strain distribution may be affected and strain localization can be intensified through the HELP mechanism owing to the different hydrogen-trapping capacities of various phases, making an early failure across martensite, ferrite or along martensite/austenite phase boundaries. However, the determination of fracture paths is mainly based on macroscopic observations of post-fracture samples [6,21], which lacks a comprehensive understanding of how hydrogen induces cracking initiates in QP steel. Hence, to reveal the critical microstructure that leads to the HE fracture and obtain a better understanding of the HE mechanism of QP steel, there is a need for a characterization of strain distribution during the deformation under hydrogen attack.

In this study, the HE susceptibility of a commercial QP980 steel was evaluated through a slow strain rate test (SSRT) in the air and hydrogen environment, and the fracture surfaces were observed via SEM. Interrupted tensile tests and transmission Kikuchi diffraction average misorientation (TKD-KAM) analysis were used to characterize the strain distribution during the HE fracture. Finally, the HE fracture mechanism of QP980 steel was explored.

2. Experimental Procedure

A commercial QP980 steel subjected to intercritical annealing treatment was used in the present study, and the chemical compositions are given in Table 1. XRD analysis was carried out using CuKa radiation at 50 keV to investigate the phase constitution. Samples for EBSD were ground and finally polished in a silica suspension (0.02 μm) to remove the mechanically damaged layers. The EBSD results were processed using HKL Channel 5 (Version 5.0.9.0, Oxford, UK) software, and the volume fractions of ferrite,

martensite and austenite were measured based on the EBSD results using ImageJ (Version 1.52, NIH) software.

Table 1. Chemical compositions (mass%) of the QP980 steel.

C	Mn	Si	Mo	Al	P	S	Fe
0.216	2.06	1.64	0.57	0.049	0.012	0.0026	Bal.

HE susceptibility was evaluated using SSRT with a strain rate of 1×10^{-5} s^{-1}. The SSRT tests were performed in air and under electrochemical hydrogen charging conditions according to ASTM G129-00. Electrochemical hydrogen charging was carried out in a 1 M NaOH solution containing 1 g L^{-1} thiourea with a constant cathodic current density of 1 mA cm^{-2}. Flat dog-bone-shaped specimens with a gauge length of 30 mm, a cross-sectional width of 6 mm and a thickness of 0.6 mm were used for SSRT, and the strain rate was set as 1×10^{-5} s^{-1}. All the specimens were abraded along the tensile direction by using 2000 grit abrasive papers before the tensile test. Each test was repeated at least three times in order to ensure the reproducibility of the measurements. Fracture surfaces of the SSRT specimens were observed using SEM. The relative plastic loss, I_δ, is defined as the HE susceptibility, where δ_H and δ_{air} are the elongation with H and without H, respectively.

$$I_\delta = \left(1 - \frac{\delta_H}{\delta_{air}}\right) \times 100\% \quad (1)$$

Electrochemical permeation (EP) tests were carried out using the Devanathan–Stachurski two-component permeation cell to evaluate the hydrogen diffusion coefficient. The membrane used for EP tests was abraded by using 2000 grit abrasive papers, and the detection side was electrochemically coated with a thin nickel layer to avoid the influence of the passive oxide layer. Then, a 0.2 M NaOH solution was introduced to the detection component. A static potential of 200 mV verse saturated calomel electrode (SCE) was applied at the detection side to remove the original hydrogen that existed in the specimen, and the current density was recorded simultaneously. When the residual current density decreased to a few nA/cm^2, the 0.2 M NaOH solution was introduced to the charging component and a cathodic current density of 10 mA/cm^2 was applied for hydrogen charging. Hydrogen passing through the membrane was recorded at the detection side during the whole charging procedure. The effective diffusion coefficient of hydrogen D_{eff} can be determined using the following equation [22]:

$$D_{eff} = \frac{L^2}{6t_{0.63}} \quad (2)$$

where L is the sample thickness and $t_{0.63}$ is the "breakthrough time", which is usually defined as the time when the transient current density is equal to 63% of the steady-state current density.

To reveal the critical microstructure that leads to the HE fracture of QP980 steel, TKD was conducted to provide nanoscale imaging of the local misorientation for deformed specimens with hydrogen charging. SSRT was conducted and intermediately terminated at approximately 4% engineering strain for the hydrogen-charged specimens. Rectangular sections were subsequently excised from the central region of the tensile specimens, and a portion was reserved for EBSD analysis. The remaining segments were subjected to mechanical and jet polishing using a solution of 10% perchloric acid ($HClO_4$) and 90% ethanol before undergoing TKD analysis. The TKD scanning was performed with a step size of 10 nm. TKD-KAM mappings were determined using nearest-neighbor points in a hexagonal grid with a threshold misorientation of 5° by using HKL Channel 5 software.

3. Results

The XRD results show that QP980 consists of martensite/ferrite and austenite phases, as indicated in Figure 1. However, due to the same body-centered cubic (bcc) structure of martensite and ferrite, it is hard to distinguish these two phases using XRD, and this issue can be resolved using EBSD discrimination based on the different dislocation density of these two phases. The EBSD band contrast (BC) image and the corresponding KAM maps of QP980 are shown in Figure 2. The austenite can be directly identified from the EBSD phase image, as indicated by the red regions in Figure 2c. In addition to the austenite phase, the bright grains observed in the IQ map and the low-KAM-value regions depicted in the KAM maps are indicative of ferrite, whereas martensite is characterized by the opposite. The quantitative analysis of phase fractions was accomplished through the following procedures: (i) the automatic identification of ferrite in BC images using ImageJ, and (ii) the manual adjustment of ferritic regions using ImageJ based on KAM images. For clarity, the ferrite is indicated by green regions in Figure 2c. The results show that the volume fractions of martensite, ferrite and austenite are 56%, 42% and 2%, respectively. Meanwhile, it can be seen that the austenite phases are mainly distributed at the grain or phase boundaries of ferrite and martensite. The EP test results are depicted in Figure 3. According to Equation (2), the apparent hydrogen diffusion coefficient of QP980 steel is calculated to be 1.3×10^{-11} m^2/s, which is similar to the values reported in the literature [7,22].

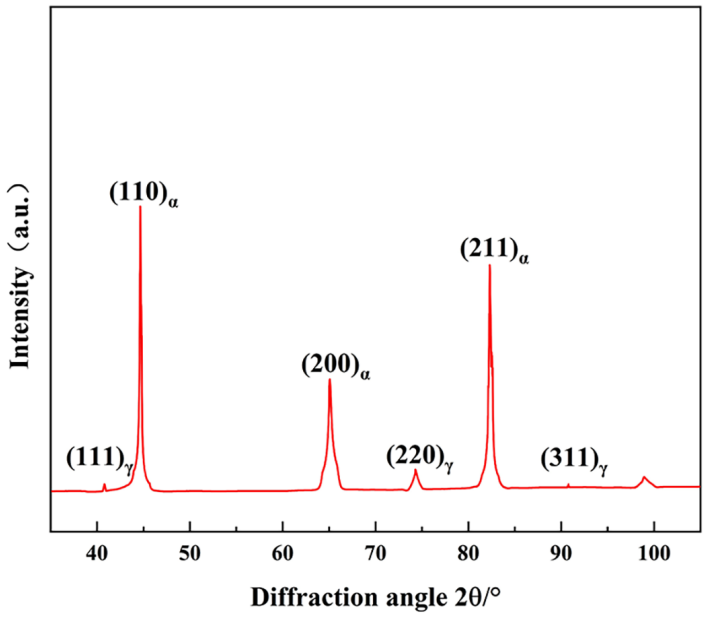


Figure 1. XRD spectra of QP980 steel.

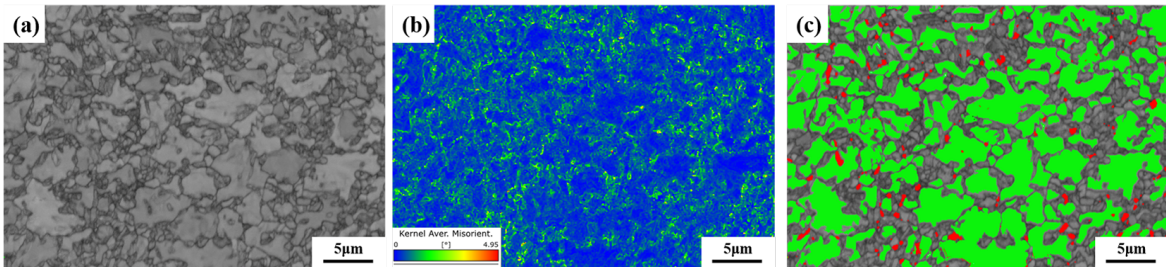


Figure 2. EBSD (**a**) BC image, (**b**) KAM maps of QP980 steel and (**c**) BC image with ferrite (green color) and austenite phases (red color) superimposed.

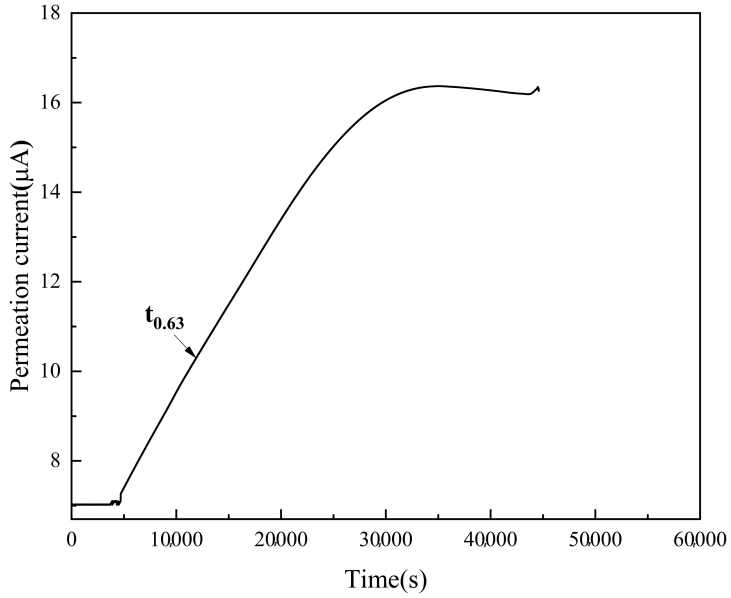


Figure 3. Typical hydrogen permeation curve of QP980 steel.

Figure 4 shows the typical SSRT engineering stress and strain curves of hydrogen-charged and -uncharged QP980 steel. It is evident that hydrogen charging leads to a significant reduction in elongation and premature fractures for QP980 steel. Meanwhile, the tensile strength of QP980 steel is also drastically reduced by hydrogen charging.

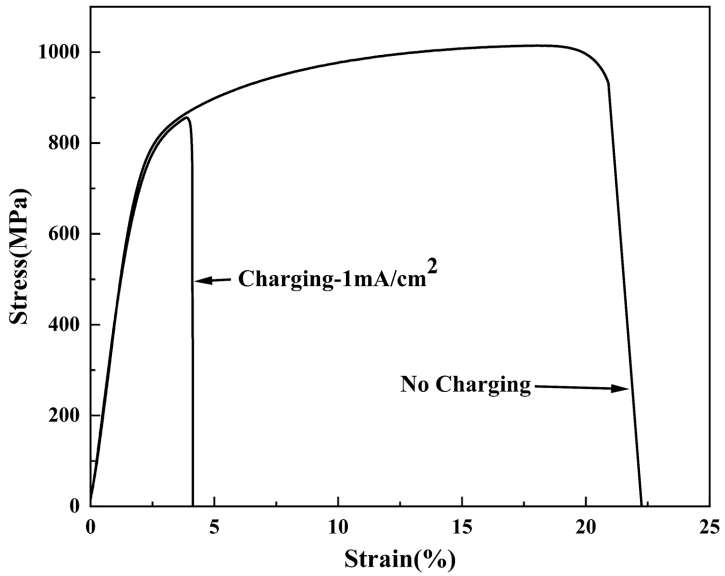


Figure 4. Typical engineering stress–strain curves of QP980 tested in an air and hydrogen environment with a strain rate of 1×10^{-5} s^{-1}.

According to Equation (1), the HE susceptibility is determined to be 78%, which indicates that QP980 suffers from severe HE susceptibility under such hydrogen charging conditions. When studying the HE of materials using SSRT, it is necessary to consider whether the whole tensile sample can be affected by hydrogen during the SSRT. The maximum diffusion distance of hydrogen (s) during the tensile test can be estimated using the following equation [23]: $s = \sqrt{2Dt}$, where D is the apparent hydrogen diffusion coefficient (1.3×10^{-11} m^2/s) and t is the total duration before the final HE fracture (4560 s). Accordingly, the value of s can be calculated as 0.34 mm, which exceeds half the thickness of the SSRT specimen, indicating that the whole tensile specimen is affected

by hydrogen during SSRT. The fracture surfaces after SSRT are indicated in Figure 5. As seen from Figure 5a, the fracture surface of the uncharged QP980 displays a dimpled morphology, with microvoid coalescence being the dominant mode of fracture. As for the hydrogen-charged sample, quasi-cleavage fracturing, which is a typical HE fracture feature of ferritic [24], martensitic [25] and austenitic steels [26], becomes the dominant fracture mode across the entire fracture surface (Figure 5b). The high-magnification fracture image of hydrogen-charged QP980 (Figure 5c) reveals that flat cleavage facets, whose sizes are smaller than the grain size, are linked by tear ridges (with a bright contrast), which is a typical characteristic of quasi-cleavage fractures. Hence, it can be concluded that a transition of the fracture mode from ductile to brittle is triggered by hydrogen attack.

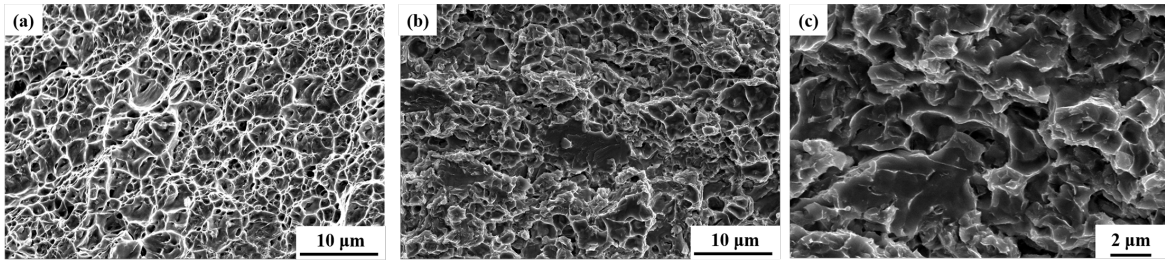


Figure 5. SEM images of fracture surfaces of (**a**) hydrogen-uncharged and (**b**,**c**) hydrogen-charged QP980 steels.

Previous studies have emphasized the crucial role of austenite in QP or martensitic steels in relation to HE fracture, as it can significantly influence the localized hydrogen distribution in steels. Hence, it is necessary to characterize the transformation of austenite during SSRT under hydrogen charging. Figure 6a displays the EBSD-BC map of the hydrogen-charged 4% strained sample with the austenite phase superimposed (red color). The EBSD phase analysis results indicate that the volume fraction of austenite is 1.9%, which closely approximates the value of the undeformed sample. Given that the 4% strain is in close proximity to the HE fracture strain of QP980 (4.7%, as shown in Figure 4), it can be inferred that there may exist minimal austenite-to-martensite transformation prior to the final hydrogen-induced cracking in QP980 steel. To enhance the HE resistance of QP980 steel, it is imperative to identify the critical microstructure that triggers the initiation of HE cracking. Therefore, the meticulous characterization of the localized strain distribution during hydrogen-charged SSRT testing, in addition to the identification of the fracture path in a post-fracture sample, is also indispensable, as it can furnish information on preferred sites for crack initiation. With the aid of TKD, which can offer a higher spatial resolution than conventional EBSD, the localized strain distribution in QP experienced with 4% hydrogen-charged tensile strain can be effectively characterized. Figure 7a presents the TKD-BC image with the austenite phase superimposed (red color), and the KAM mapping of the region marked by yellow dotted lines is also included. By combining the IQ and KAM images, this method is capable of accurately distinguishing between the ferrite and martensite phases. Correspondingly, KAM profiles from austenite to martensite (solid black line in Figure 7a) and from martensite to ferrite (red dashed line in Figure 7a) can be obtained, while the phase interfaces are also indicated, as shown in Figure 7b. It can be seen that the KAM values of martensite are much higher than those of austenite and ferrite. Meanwhile, the KAM values in the regions adjacent to the interfaces do not exhibit a significant increase compared to the surrounding matrix. Generally, the KAM maps can be used to reflect the degree of strain localization, and sites with high KAM values are usually indicative of high strain localization where cracking tends to occur, and vice versa [27,28]. Hence, it can be preliminarily inferred that the phase interfaces are not the preferred hydrogen-induced cracking sites. It is also noted that the maximum KAM value in the martensite adjacent to austenite is relatively lower than that in the martensite adjacent to ferrite, which means that hydrogen induced cracking may be more likely to initiate in the martensite adjacent to ferrite.

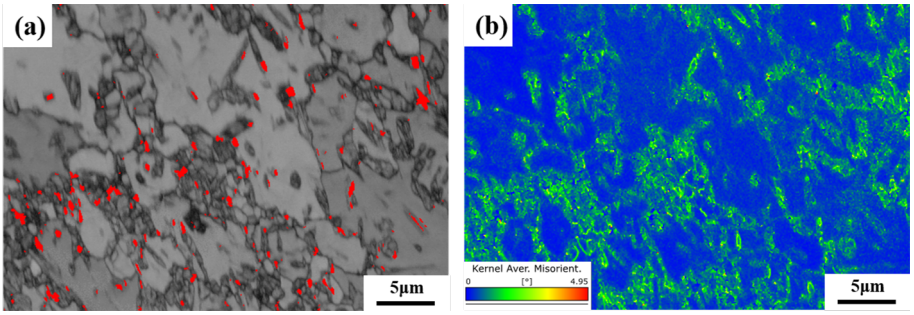


Figure 6. EBSD (**a**) BC and (**b**) KAM maps of QP980 steel after being subjected to 4% engineering strain under hydrogen charging.

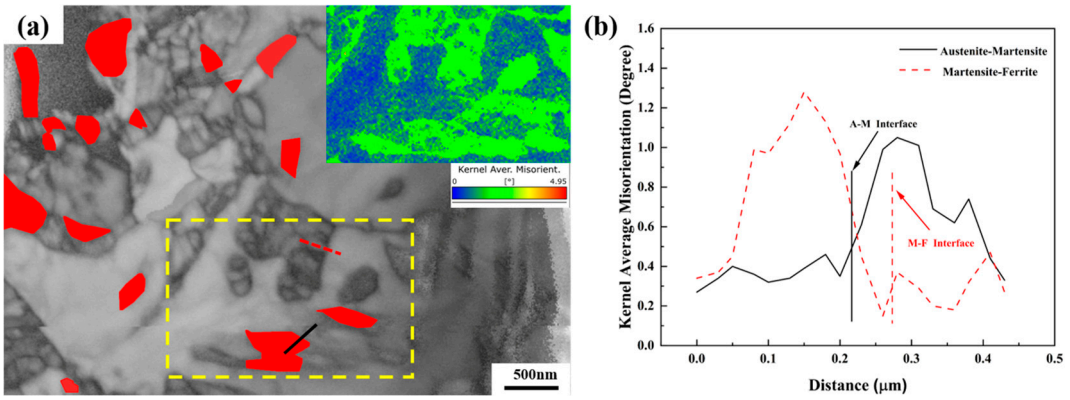


Figure 7. TKD images of QP980 steel after being subjected to 4% engineering strain under hydrogen charging. (**a**) TKD-BC image and KAM mapping of the region marked by yellow dotted lines. (**b**) KAM profiles. (For interpretation of the references to color in this figure legend, the reader is referred to the web version of this article.).

4. Discussion

The HE susceptibility results indicate that QP980 steel suffers from a severe HE, and the fracture mode transforms from ductile dimpling to brittle quasi-cleavage fracturing under the attack of hydrogen (Figure 5). The EBSD analysis results show that transformation from austenite to martensite can rarely occur at a strain very close to the HE fracture strain, which may be attributed to the following aspects: on the one hand, the small size of austenite (Figure 1) [29] and the C enrichment in austenite during partitioning ensure the high mechanical stability of austenite; on the other hand, the HE fracture strain is relatively low (about 4.7%), potentially falling below the critical strain required for martensite transformation [30]. Correspondingly, as for the hydrogen-induced cracking initiation of QP980, the viewpoint that "austenite serves as a source of hydrogen and accelerates HE fracture" may not be applicable in this study. Combined with the TKD-KAM results indicating that the strain localization at the martensite–austenite interface is not prominent, it can be concluded that the martensite–austenite interface is not the preferred initiation site of hydrogen-induced cracking.

In addition to the martensite–ferrite interface, the ferrite–martensite phase can also serve as a potential site for cracking initiation. It has been reported that ferrite–martensite interface decohesion is prone to occur during deformation without the attack of hydrogen due to the strength mismatch between ferrite and martensite through the void nucleation mechanism [31]. As for the QP980 steel used in this study, the volume fraction of martensite is much higher and most of the ferrite grains are well covered by martensite (Figure 2), which is considered to decrease the tendency of ferrite–martensite interfacial cracking owing to the restricting effect of hard martensite [32]. Meanwhile, it is widely recognized that martensite exhibits significant sensitivity to HE, and HE cracking of high-strength martensitic steels may even occur within the elastic regime [33]. Combined with the

TKD-KAM results indicating that the degree of strain localization at the ferrite–martensite interface is much lower than that in martensite (Figure 7b), it can be deduced that hydrogen-induced cracking is apt to initiate in martensite rather than at the ferrite–martensite interface. A similar result was reported by Motomichi Koyama et al., who demonstrated that HE cracking initiates in the martensite region in martensite–ferrite dual-phase steel [27]. It is also noted that the strain localization in martensite adjacent to austenite is relatively lower than that in martensite adjacent to ferrite, which can be understood as follows: generally, the presence of hydrogen is known to induce strain localization during deformation through the mechanism of HELP, and the extent of strain localization is directly proportional to the concentration of hydrogen. Austenite, which has been proven to be a hydrogen-trapping site via scanning Kelvin probe force microscopy [34] and three-dimensional atom probes [14], is considered to reduce the hydrogen content of the surrounding martensite. Meanwhile, the EBSD analysis demonstrates that austenite within QP980 remains stable even in close proximity to the HE fracture. Consequently, austenite is regarded as a stable hydrogen trapping site, which can effectively mitigate the hydrogen accumulation in its surrounding martensite. Finally, the hydrogen-induced strain localization in martensite adjacent to austenite can be alleviated, resulting in a relatively lower KAM value compared to that of martensite adjacent to ferrite (Figure 7b).

According to the above analysis of the TKD-KAM results, it can be concluded that the martensite adjacent to ferrite is the most optimal site for hydrogen-induced cracking initiation of QP980, and the HE cracking initiation in martensite can be understood as follows: generally, lath boundaries are considered as barriers to dislocation motion [35], leading to dislocation pile-ups at lath boundaries and the resulting severe strain localization in martensite (Figure 7b), and the strain localization can be enhanced by the presence of hydrogen owing to the HELP mechanism. Meanwhile, accompanied by strain localization, hydrogen tends to redistribute and segregate at lath boundaries, and this hydrogen accumulation can be accentuated by dislocation-assisted convection as proposed by the HELP mechanism. Finally, when the hydrogen concentration at lath boundaries exceeds the threshold value for HE fracture, an initiation of hydrogen-induced cracking at lath boundaries can occur through the HEDE mechanism [33].

Once the crack initiates and propagates further, the stress concentration at the crack tip increases accordingly, accompanied by hydrogen accumulation in the vicinity of the crack tip. Subsequently, the transformation from austenite to martensite near the crack tip can be triggered by high levels of stress and hydrogen concentration (hydrogen is deemed to decrease the stacking fault energy of austenite and promote its transformation into martensite), which results in hydrogen liberation from austenite and subsequent accumulation at martensite–austenite interfaces. Ultimately, HE cracks can propagate along the interfaces between martensite and austenite through the HEDE mechanism. Although the previous literature has reported on the propagation of cracks along martensite–austenite interfaces [14], such cracks were not directly characterized in the current experiments. Meanwhile, cracking propagation along the martensite–ferrite interface can also occur under the attack of hydrogen when considering the following factors: (i) hydrogen, which has been proven to decrease the elastic interactions between dislocations through TEM observations [36], can decrease the back stress within ferrite imposed by martensite [37], which promotes dislocation pile-ups and the resulting strain localization at the interfaces; (ii) then, void nucleation can be intensified under the synergistic action of stress concentration around crack tips, strain localization at the interface and the HESIV mechanism, resulting in crack propagation along the martensite–ferrite interface. Furthermore, when HE cracking encounters ferrite, the high hydrostatic stresses near the crack tip can cause an accumulation of hydrogen in the ferrite, which can also result in quasi-cleavage cracking through ferrite under the synergistic action of HELP and HESIV [38]. Finally, the aforementioned hydrogen-induced brittle cracks are linked during the final separation, forming quasi-cleavage fracture features consisting of small cleavage facets and tear ridges, as indicated in Figure 5b.

In contrast to the previous perspective that the austenite–martensite interface [39] or blocky austenite [5] represents the preferred site for the initiation of HE cracking of QP steel, our results indicate that HE cracking is more likely to initiate in martensite adjacent to ferrite, primarily due to the high mechanical stability of austenite and the resultant stable hydrogen-trapping capacity of austenite in the QP980 steel used in this study. Our findings suggest that to further improve the HE resistance of QP steel with stable austenite, it is necessary to consider introducing effective hydrogen-trapping sites (such as carbides, film austenite) into martensite, which is deemed to be beneficial for increasing the resistance against hydrogen-induced cracking initiation in martensite.

5. Conclusions

The HE behavior of QP980 steel has been studied. The conclusions can be made as follows:

1. The EBSD analysis results indicate that QP980 steel consists of martensite, ferrite, and austenite with volume fractions of 56%, 42%, and 2%, respectively.
2. QP980 exhibits a severe HE susceptibility of 78%, and the fracture mode under hydrogen charging is quasi-cleavage fracturing.
3. Strain-induced transformation from austenite to martensite can rarely occur at a strain close to the HE fracture strain of QP980 due to the high mechanical stability of austenite.
4. The TKD-KAM results show that strain localization is most pronounced in martensite adjacent to ferrite, and hydrogen-induced cracking is considered to initiate from this area under the synergistic action of HELP and HEDE mechanisms.

Author Contributions: Conceptualization, L.Z.; Methodology, Z.L.; Validation, C.M.; Investigation, L.Z., C.M. and Z.L.; Resources, C.M.; Writing—original draft, L.Z.; Writing—review and editing, A.Z. and Y.F.; Visualization, A.Z. and Y.F.; Supervision, A.Z. All authors have read and agreed to the published version of the manuscript.

Funding: This research was funded by the National Natural Science Foundation of China (Grant No. 52001282) and the Young Scientist Support Project of Henan Province (Grant No. 2022HYTP015).

Institutional Review Board Statement: Not applicable.

Informed Consent Statement: Not applicable.

Data Availability Statement: The raw/processed data required to reproduce these findings cannot be shared at this time due to technical or time limitations. They will be shared upon request.

Conflicts of Interest: The authors declare no conflict of interest.

References

1. Carpio, M.; Calvo, J.; García, O.; Pedraza, J.P.; Cabrera, J.M. Heat Treatment Design for a QP Steel: Effect of Partitioning Temperature. *Metals* **2021**, *11*, 1136. [CrossRef]
2. Li, Y.; Li, W.; Liu, W.; Wang, X.; Hua, X.; Liu, H.; Jin, X. The austenite reversion and co-precipitation behavior of an ultra-low carbon medium manganese quenching-partitioning-tempering steel. *Acta Mater.* **2018**, *146*, 126–141. [CrossRef]
3. Salehiyan, D.; Samei, J.; Amirkhiz, B.S.; Hector, L.G.; Wilkinson, D.S. Microstructural Evolution During Deformation of a QP980 Steel. *Metall. Mater. Trans. A* **2020**, *51*, 4524–4539. [CrossRef]
4. Kim, S.; Lee, J.; Barlat, F.; Lee, M.-G. Transformation kinetics and density models of quenching and partitioning (Q&P) steels. *Acta Mater.* **2016**, *109*, 394–404. [CrossRef]
5. Zhu, X.; Zhang, K.; Li, W.; Jin, X. Effect of retained austenite stability and morphology on the hydrogen embrittlement susceptibility in quenching and partitioning treated steels. *Mater. Sci. Eng. A* **2016**, *658*, 400–408. [CrossRef]
6. Wang, Z.; Luo, Z.C.; Huang, M.X. Revealing hydrogen-induced delayed fracture in ferrite-containing quenching and partitioning steels. *Materialia* **2018**, *4*, 260–267. [CrossRef]
7. Zhou, P.; Li, W.; Zhao, H.; Jin, X. Role of microstructure on electrochemical hydrogen permeation properties in advanced high strength steels. *Int. J. Hydrogen Energy* **2018**, *43*, 10905–10914. [CrossRef]
8. Beachem, C.D. A new model for hydrogen-assisted cracking (hydrogen "embrittlement"). *Metall. Trans.* **1972**, *3*, 441–455. [CrossRef]
9. Oriani, R.A. A mechanistic theory of hydrogen embrittlement of steels. *Berich. Bunsen. Gesell.* **1972**, *76*, 848–857. [CrossRef]

10. Lynch, S.P. Environmentally assisted cracking: Overview of evidence for an adsorption-induced localised-slip process. *Acta Metall.* **1988**, *36*, 2639–2661. [CrossRef]
11. Nagumo, M.; Nakamura, M.; Takai, K. Hydrogen thermal desorption relevant to delayed-fracture susceptibility of high-strength steels. *Metall. Mater. Trans. A* **2001**, *32*, 339–347. [CrossRef]
12. Martin, M.L.; Fenske, J.A.; Liu, G.S.; Sofronis, P.; Robertson, I.M. On the formation and nature of quasi-cleavage fracture surfaces in hydrogen embrittled steels. *Acta Mater.* **2011**, *59*, 1601–1606. [CrossRef]
13. Nagao, A.; Martin, M.L.; Dadfarnia, M.; Sofronis, P.; Robertson, I.M. The effect of nanosized (Ti, Mo) C precipitates on hydrogen embrittlement of tempered lath martensitic steel. *Acta Mater.* **2014**, *74*, 244–254. [CrossRef]
14. Fan, Y.H.; Zhang, B.; Yi, H.L.; Hao, G.S.; Sun, Y.Y.; Wang, J.Q.; Han, E.H.; Ke, W. The role of reversed austenite in hydrogen embrittlement fracture of S41500 martensitic stainless steel. *Acta Mater.* **2017**, *139*, 188–195. [CrossRef]
15. Elsayed, H.; Drexler, A.; Warchomicka, F.; Traxler, I.; Domitner, J.; Galler, M.; Vallant, R.; Sommitsch, C. Resistance of Quench and Partitioned Steels Against Hydrogen Embrittlement. *J. Mater. Eng. Perform.* **2023**, *32*, 5186–5200. [CrossRef]
16. Li, X.; Zhang, J.; Chen, J.; Shen, S.; Yang, G.; Wang, T.; Song, X. Effect of aging treatment on hydrogen embrittlement of PH 13-8 Mo martensite stainless steel. *Mater. Sci. Eng. A* **2016**, *651*, 474–485. [CrossRef]
17. Yang, J.; Huang, F.; Guo, Z.; Rong, Y.; Chen, N. Effect of retained austenite on the hydrogen embrittlement of a medium carbon quenching and partitioning steel with refined microstructure. *Mater. Sci. Eng. A* **2016**, *665*, 76–85. [CrossRef]
18. Park, Y.; Maroef, I.; Landau, A.; Olson, D. Retained austenite as a hydrogen trap in steel welds. *Weld. J. N. Y.* **2002**, *81*, 27-S.
19. Zhu, X.; Li, W.; Zhao, H.; Wang, L.; Jin, X. Hydrogen trapping sites and hydrogen-induced cracking in high strength quenching & partitioning (Q&P) treated steel. *Int. J. Hydrogen Energ.* **2014**, *39*, 13031–13040. [CrossRef]
20. Yang, Y.; Mi, Z.; Liu, S.; Li, H.; Li, J.; Jiang, H. The Impact of Strain Heterogeneity and Transformation of Metastable Austenite on Springback Behavior in Quenching and Partitioning Steel. *Metals* **2018**, *8*, 432. [CrossRef]
21. Wang, Z.; Wan, Z.; Zhou, Y.; Chen, X.; Zhang, J.; Huang, T.; Kong, X.; Ou, C.; Li, J. Investigation for enhancing the resistance of H-induced delayed cracking for martensitic steel by quenching tempering and quenching partitioning: Influence of microstructure on hydrogen embrittlement and cracking behavior. *Int. J. Hydrogen Energy* **2022**, *47*, 27250–27265. [CrossRef]
22. Zhao, Z.; Liu, M.; Zhou, Q.; Li, M. Hydrogen permeation behavior of QP1180 high strength steel in simulated coastal atmosphere. *J. Mater. Res. Technol.* **2022**, *18*, 2320–2330. [CrossRef]
23. Lynch, S. Hydrogen embrittlement phenomena and mechanisms. *Corros. Rev.* **2012**, *30*, 105–123. [CrossRef]
24. Merson, E.; Myagkikh, P.; Poluyanov, V.; Dorogov, M.; Merson, D.; Vinogradov, A. The fundamental difference between cleavage and hydrogen-assisted quasi-cleavage in ferritic materials revealed by multiscale quantitative fractographic and side surface characterization. *Mater. Sci. Eng. A* **2021**, *824*, 141826. [CrossRef]
25. Fan, Y.H.; Zhao, H.L.; Weng, K.R.; Ma, C.; Yang, H.X.; Dong, X.L.; Guo, C.W.; Li, Y.G. The role of delta ferrite in hydrogen embrittlement fracture of 17-4 PH stainless steel. *Int. J. Hydrogen Energy* **2022**, *47*, 33883–33890. [CrossRef]
26. Fan, Y.H.; Cui, F.; Lu, L.; Zhang, B. A nanotwinned austenite stainless steel with high hydrogen embrittlement resistance. *J. Alloys Compd.* **2019**, *788*, 1066–1075. [CrossRef]
27. Koyama, M.; Tasan, C.C.; Akiyama, E.; Tsuzaki, K.; Raabe, D. Hydrogen-assisted decohesion and localized plasticity in dual-phase steel. *Acta Mater.* **2014**, *70*, 174–187. [CrossRef]
28. Fan, Y.H.; Zhang, B.; Wang, J.Q.; Han, E.H.; Ke, W. Effect of grain refinement on the hydrogen embrittlement of 304 austenitic stainless steel. *J. Mater. Sci. Technol.* **2019**, *35*, 2213–2219. [CrossRef]
29. Xiong, X.C.; Chen, B.; Huang, M.X.; Wang, J.F.; Wang, L. The effect of morphology on the stability of retained austenite in a quenched and partitioned steel. *Scr. Mater.* **2013**, *68*, 321–324. [CrossRef]
30. De, A.K.; Speer, J.G.; Matlock, D.K.; Murdock, D.C.; Mataya, M.C.; Comstock, R.J. Deformation-induced phase transformation and strain hardening in type 304 austenitic stainless steel. *Metall. Mater. Trans. A* **2006**, *37*, 1875–1886. [CrossRef]
31. Kadkhodapour, J.; Butz, A.; Ziaei Rad, S. Mechanisms of void formation during tensile testing in a commercial, dual-phase steel. *Acta Mater.* **2011**, *59*, 2575–2588. [CrossRef]
32. Saeidi, N.; Ashrafizadeh, F.; Niroumand, B.; Barlat, F. EBSD Study of Damage Mechanisms in a High-Strength Ferrite-Martensite Dual-Phase Steel. *J. Mater. Eng. Perform.* **2015**, *24*, 53–58. [CrossRef]
33. Nagao, A.; Smith, C.D.; Dadfarnia, M.; Sofronis, P.; Robertson, I.M. The role of hydrogen in hydrogen embrittlement fracture of lath martensitic steel. *Acta Mater.* **2012**, *60*, 5182–5189. [CrossRef]
34. Wang, G.; Yan, Y.; Yang, X.; Li, J.; Qiao, L. Investigation of hydrogen evolution and enrichment by scanning Kelvin probe force microscopy. *Electrochem. Commun.* **2013**, *35*, 100–103. [CrossRef]
35. Du, C.; Hoefnagels, J.P.M.; Vaes, R.; Geers, M.G.D. Block and sub-block boundary strengthening in lath martensite. *Scr. Mater.* **2016**, *116*, 117–121. [CrossRef]
36. Ferreira, P.J.; Robertson, I.M.; Birnbaum, H.K. Hydrogen effects on the interaction between dislocations. *Acta Mater.* **1998**, *46*, 1749–1757. [CrossRef]
37. He, J.; Fukuyama, S.; Yokogawa, K.; Kimura, A. Effect of Hydrogen on Deformation Structure of Inconel 718. *Mater. Trans. JIM* **1994**, *35*, 689–694. [CrossRef]

38. Neeraj, T.; Srinivasan, R.; Li, J. Hydrogen embrittlement of ferritic steels: Observations on deformation microstructure, nanoscale dimples and failure by nanovoiding. *Acta Mater.* **2012**, *60*, 5160–5171. [CrossRef]
39. Liu, Q.; Zhou, Q.; Venezuela, J.; Zhang, M.; Atrens, A. The role of the microstructure on the influence of hydrogen on some advanced high-strength steels. *Mater. Sci. Eng. A* **2018**, *715*, 370–378. [CrossRef]

Disclaimer/Publisher's Note: The statements, opinions and data contained in all publications are solely those of the individual author(s) and contributor(s) and not of MDPI and/or the editor(s). MDPI and/or the editor(s) disclaim responsibility for any injury to people or property resulting from any ideas, methods, instructions or products referred to in the content.